Synthesis and Characterization of CSH/CS/n-HA Composite Scaffold for Bone Tissue Engineering

Chunhua Gong
Guangdong Pharmaceutical University
Haixia Tang
Guangdong Pharmaceutical University
Yanbo Wu
Ministry of Agriculture
Juan Guo
Ministry of Agriculture
Ruixue Guo
Ministry of Agriculture
yongguang bi (biyongguang2002@163.com)
Guangdong Pharmaceutical University

Research Article

Keywords: CSH/CS/n-HA composite scaffold, Compressive strength, Biocompatibility, Biodegradation, Bone tissue engineering

Posted Date: May 26th, 2021

DOI: https://doi.org/10.21203/rs.3.rs-552177/v1

Abstract

In this paper, chitosan/hydroxyapatite (CS/n-HA) were synthesized by ultrasound-assisted precipitation combined with inverse crosslinking-emulsion method. In order to obtain a scaffold material with excellent properties, Calcium sulfate hemihydrate (CSH) were combined with CS-HA obtained CSH/CS/n-HA composite scaffold via setting citric acid as solidifying liquid, which possessed better biodegradability, bioactivity, mechanical properties. The physicochemical, morphological properties of scaffolds were characterized by FTIR, XRD and TFSEM. In addition, explored were the mechanical, degradable, biocompatibility and iron release properties. The mechanical strength study indicated that the compressive strength of the porous composite scaffold was influenced by adding an appropriate amount of CS/n-HA composite microspheres. It was proved that the composite scaffold with 6% CS/n-HA content obtained the highest mechanical strength (17.46±1.29 MPa). The results illustrated that the composite scaffold possessed biodegradability and can form hydroxyapatite by dynamic balance of Ca and P elements. The hemolysis tests demonstrate that materials are non-hemolytic and have good blood compatibility. Therefore, the developed composite scaffolds are safe medical inorganic materials, which can potentially be applied in bone tissue engineering.

1. Introduction

Skeleton is the hard organ of vertebrates with hierarchical structure, which mainly composed of inorganic phase (such as nano-hydroxyapatite) and organic phase (such as collagen). Skeleton has excellent mechanical properties, and also the source of hematopoietic cells and stem cells. It can protect important organs, store and release ions like calcium, exercise, support muscles and so on [1–3]. Therefore, it is important that the bone tissues are integrated and healthy. To date, there are as many as 10 million patients worldwide suffering from bone defects due to improper treatment of fractures and fractures, severe trauma, infection, bone tumors, etc. Bone defect is a common disease, mainly due to local bone loss caused by trauma and disease (such as infection, tumor, etc.) and require amount of medical resources [4, 5]. For the repair of bone defects, due to the significant limitations of traditional treatments such as bone grafting, the search for ideal bone graft replacement materials has become a research hotspot. Ideal bone scaffolds for bone tissue engineering should exist interconnected porous structure, adequate mechanical properties, excellent biocompatibility, and osteoinductivity [6, 7].

Hydroxyapatite (hydroxyapatite, $Ca_{10}(PO_4)6(OH)_2$) belongs to the apatite family and is one of the most common forms of CaP. Nano-hydroxyapatite, the main inorganic component of natural bone tissue, is often used in bone tissue engineering owing to its good biocompatibility, osteoconductivity and osteogenic capacity [8–11], low in immunogenicity and the capability to bind to hard tissue [12–14]. At present, the preparation methods of hydroxyapatite mainly include: (1) dry method, (2) wet method (mainly coprecipitation method, sol-gel method, emulsion method, hydrolysis method and hydrothermal method), (3) Alternating energy input methods (mainly microwave assisted, ball milling, sonochemistry and other methods) can be used to prepare hydroxyapatite particles of different shapes and sizes [15–19]. However, hydroxyapatite materials have difficulties in forming and easy to agglomerate, and irregular

or high-density particles usually cause inflammation, which limits their application in bone tissue engineering. It is well known that HA combined with organic polymer not only improve the mechanical properties of composite scaffold but also strengthen the biocompatibility of material.

Chitosan (($C_6H_{11}NO_4$)N) is a semi-synthetically derived polymer obtained by partial N-deacetylation of chitin, which is the second most abundant polymer in nature [20, 21]. It is widely used in the treatment of water quality, agriculture, food, cosmetics and biomedical applications, and has a wide range of applications, due to its non-toxicity, biocompatibility, biodegradability, antibacterial and emulsifying properties [22–25]. Chitosan has become a new type of research-oriented biomedical material owing to its low toxicity, biocompatibility and biodegradability [26]. The previous literature has shown that CS and its derivatives accompanied by HA will enhance materials bioactivity [27]. Among the hydrophilic semi-synthetic materials, chitosan has shown outstanding properties as tissue supporting materials [28–30].

Calcium sulfate hemihydrate ($CaSO_4·0.5H_2O$), commonly known as "Paris stucco", is an surgical grade calcium sulphate cement that does not cause inflammatory reactions due to its good biocompatibility and has bone repairing ability. It promotes bone healing and can be used to fill areas of bone defects. At present, calcium sulfate hemihydrate has long been used as a substitute for bone grafting [31–33]. At the same time, the use of inorganic cement calcium sulfate hemihydrate can overcome the migration problems of granular materials [34].

In the present work, the precursor materials from nano-hydroxyapatite and chitosan/hydroxyapatite composite microspheres were prepared using ultrasonic assisted chemical precipitation and reversed-emulsification cross-linking method, which were used to increase the compressive strength of composite scaffolds in subsequent experiments. A porous hemihydrate calcium CSH/CS/n-HA composite scaffold was prepared by combining chitosan/hydroxyapatite composite microspheres and calcium sulfate hemihydrate in different ratios. The content of doping CS/n-HA on the mechanical property were detected using a universal tensile testing machine. Additionally, the degradability of composite microspheres and property of iron release were investigated. Subsequently, the in vitro blood compatibility of n-HA, CS/n-HA, CSH/CS/n-HA and calcium sulfate hemihydrate/chitosan/hydroxyapatite composites were investigated by in vitro red blood cell hemolysis test. Through the above research, in order to obtain a new bone graft replacement material that is safe, non-toxic, and has osteogenic ability and anti-infective ability, which provides a new solution for the treatment of bone defects.

2. Results And Discussion

2.1 FT-IR analysis

FT-IR analysis was carried out to verify the conversion between n-HA, CS and CSH in the reaction process, as shown in Fig. 1(a). For n-HA, the characteristic peaks of PO_4^{3-} are at 473cm^{-1}, 567 cm^{-1}, 602 cm^{-1}, 962 cm^{-1}, 1042 cm^{-1} and 1095 cm^{-1}, which were owing to the P-O stretching vibration of PO_4^{3-} [39–41]. In addition, the peaks at 631 cm^{-1} and 3571 cm^{-1} were ascribed to the OH^- of hydroxyapatite [42]. The

spectrum of CS showed the characteristic peaks at 3444 cm^{-1} (overlap of O-H and N-H stretch), 1654 cm^{-1} (NH-CO stretch) and 1589 cm^{-1} (N-H bend), respectively [43]. The absorption peaks at 894 cm^{-1}, 1083 cm^{-1} and 1153 cm^{-1} originated from the glycosyl of chitosan. Figure 1a was the infrared spectra of CS/n-HA composite microspheres (c). The IR spectra of CSH/CS/n-HA was shown in Fig. 1b. The characteristic absorption peaks of SO_4^{2-} were observed at 602 and 1143 cm^{-1}. The peak of 3404 cm^{-1} was caused by the symmetric and antisymmetric stretching of H_2O.

2.2 XRD analysis

Figure 2a shows the XRD pattern of the n-HA material. As shown in the figure, diffraction peaks appeared at positions of 10.8°, 25.9°, 31.8°, 32.2°, 32.9°, 39.8°, 46.7°, 49.4°, 53.1°, and 64.1°, which were consistent with characteristic diffraction peaks of hydroxyapatite standards proving the successful preparation of hydroxyapatite. Figure 2b revealed that the XRD pattern of pure CS powder showed characteristic diffraction peaks at only 10.7° and 20° at 2Θ [44, 45]. From Fig. 2b, the characteristic diffraction peaks of CS and n-HA appeared in the spectrum of CS/n-HA composite microspheres, and the intensity of the characteristic diffraction peak of CS uplift was weakened which were ascribed to the Schiff base reaction reducing the crystallinity of CS during cross-linking [46]. Comparing the diffraction peaks of n-HA (a), the peak shape of the characteristic diffraction peak of n-HA was still obvious in the XRD pattern of CS/n-HA composite microspheres (eg 2Θ = 25.9°, 31.8°, 32.2°, 32.9°, 39.8°), but significantly weakened, indicating that the crystallinity of n-HA was reduced after the two materials combined. Figure 2c is an XRD pattern of a CSH/CS/n-HA composite. The overall intensity of the diffraction peaks of the CSH/CS/n-HA composites was weakened.

2.3 Morphology analysis

SEM image of n-HA microsphere prepared by ultrasound-assisted chemical precipitation method showed that the synthesized n-HA exhibited a rod-like morphology with a uniform particle size distribution (Fig. 3a). As can be seen from Figs. 4a, b, more holes were observed on the surface of the CSH/CS/n-HA composite scaffold, but the distribution was uneven and irregular. According to the results of electron micrograph, Fig. 4c showed that calcium sulfate hemihydrate was a material of sheet structure. At the same time, the two materials were successfully combined according to the TFSEM image of the composite scaffold indicating that more CS/n-HA composite microspheres were embedded in the flake calcium sulfate hemihydrate and embedded in the scaffold (Figs. 4d, e, f). Therefore, an intuitive morphological characterization can verify the successful preparation of porous CSH/CS/n-HA composite scaffolds.

2.4 Mechanical strength study

The mechanical strength results indicated that the addition of an appropriate amount of CS/n-HA composite microspheres could effectively increase the maximum compressive strength of the porous composite stent. Briefly, the five sets of samples were subjected to a compression test using a universal

testing machine, and the results were shown in Table 1. Compared with CSH scaffolds (CS/n-HA content of 0%), the maximum compressive strength of the scaffolds increased with an increase of CS/n-HA content (2%, 4% and 6%). When the CS/n-HA content was 6%, the compressive strength of the composite scaffold reaches the highest, which is 17.46 ± 1.29 MPa. When the CS/n-HA content was increased to 8%, the compressive strength of the stent decreased, even lower than the pure CSH scaffold.

Table 1
Comparison of compressive strength of porous composite scaffolds

Group	Number	CS/n-HA content (%)	Maximum compressive strength (MPa)
1	3	0	11.02 ± 0.52
2	3	2	12.16 ± 1.03
3	3	4	13.32 ± 0.58
4	3	6	17.46 ± 1.29
5	3	8	10.92 ± 0.67

2.5 In-vitro degradation

Biodegradation is a vital factor to assess whether the scaffold can be implanted in human body which also should possess a controllable speed, biocompatible and non-toxic property. In this experiment, five groups of CSH/CS/n-HA composite scaffolds (cylinder, Φ10 mm×10 mm) with CS/n-HA content of 0%, 2%, 4%, 6% and 8% were immersed in SBF solution to initially evaluate its degradation performance. The weight was taken every 24 h and the fresh SBF solution was replaced. The daily weight variable rate of the stent samples with increasing soaking time is shown in Fig. 5a. During the experiment, the five groups of stents were immersed until the 15th day, and the remaining weight had dropped to 1–4% of the initial weight until the simulated body fluid immersion experiment was stopped. As shown in Fig. 5a, the trend line of the daily weight loss rate of the CSH stent decreases day by day, with no obvious fluctuations. In general, there was no significant difference in the trend between the other four groups of stent samples, and the fluctuations in the first 5 days were larger. After the sixth day, the daily weight loss rate tended to change smoothly and decreased as time flows. It was speculated that this was a tightly structured scaffold formed by the exquisite CSH powder attributed to the addition of CS/n-HA composite microspheres so that the gap of the CSH/CS/n-HA composite scaffold was increased, which was more conducive to the entry of the SBF solution into the scaffold promoting the degradation of the stent.

2.6 Concentration change of Ca in soaking liquid

The variation of Ca^{2+} concentration with the immersion time was observed as shown in Fig. 5c. The EDTA complexometric titration method was used to determine the concentration of calcium ions in SBF soaking solution of the five groups of samples, and the fresh SBF solution was set as the control (x = 0, y = 0.0026). During the immersion experiment, Ca^{2+} was released from the 5 sample holders, and the Ca^{2+}

concentration was always higher than that of the SBF stock solution. However, the Ca^{2+} concentration of the soaking solution decreased day by day compared with the sample before immersion. The data shows that there is no significant difference in the trend line of Ca^{2+} concentration with time compared with the other four sets of composite scaffolds with different CS/n-HA content. Therefore, it can be considered that the Ca^{2+} released in the solution is mainly derived from the material Calcium sulfate hemihydrate and calcium sulfate dihydrate.

2.7 Concentration change of phosphorus in soaking liquid

The reagent blank was set as the control, and the PO_4^{3-} solution with different concentration gradients was taken at 319 nm, and the absorbance values were determined by ultraviolet-visible spectrophotometer. The standard curve is fitted using the software Origin. The results are shown in Fig. 6. Within the measured concentration range, the fitting yields a linear equation y = 0.13036x with a correlation coefficient r of 0.99957.

The PO_4^{3-} concentration change of the daily SBF soaking solution can be determined by the phosphorus-molybdenum yellow ultraviolet-visible spectrophotometry and determined by the above linear equation. As shown in Fig. 5d, it is a trend diagram of phosphorus content in SBF soaking solution with time. The SBF stock solution was set as the control (x = 0, y = 5.5036). In the process of simulating body fluid soaking, the concentration of PO_4^{3-} was always lower than that of the SBF stock solution before the stent sample was completely degraded, and the steady decrease trend was observed. The scaffold sample was degraded to the 15th day, and the concentration of PO_4^{3-} was increased to almost the same level as that in the SBF stock solution.

During the simulated experiment, the Ca^{2+} concentration released in the soaking solution decreased day by day, the PO_4^{3-} concentration also decreased steadily, with white sediment at the bottom of beakers, as shown in Fig. 7a. It is used and verified by means of infrared and X-ray diffraction analysis, and the results are shown in Figs. 7b, c. The FT-IR spectrum showed characteristic absorption peaks of phosphate (PO_4^{3-}) at positions 565 cm^{-1}, 603 cm^{-1} and 1043 cm^{-1}. Figure 7c showed the XRD pattern of the uncalcined deposits. The crystallinity is low, and the diffraction peaks of hydroxyapatite are still observed at 25.9°, 31.8°, 49.4° and 53.1°. It is speculated that during the soaking process, hydroxyapatite was formed due to the dynamic changes of Ca^{2+} and PO_4^{3-}.

2.8 In-vitro hemolysis study

The hemolysis rates of the different concentrations of n-HA, CS/n-HA and CSH/CS/n-HA suspensions were less than 5% in accordance with the Standard Practice of American Society for Testing and Materials Designation (ASTM:F 756-00), when the hemolysis rate is below 2% and 2% between 5%, those materials were viewed as non-hemolytic and slightly hemolytic, respectively. The results of in-vitro hemolysis experiments are shown in Fig. 8. Overall, the hemolysis rate of the three materials increased

slightly with the increase of concentration of the suspension, and the maximum concentration of material hemolysis rate is less than 5%, indicating that no hemolysis occurs in the three concentrations of the material in the experimental concentration range, which meets the hemolysis experiment requirements and national standards of medical materials.

2.9 Discussion

FTIR spectra of CS/n-HA composite microspheres (Fig. 1a), which compared with the spectra of n-HA and pure CS powder. Some characteristic peaks of n-HA and CS overlap on spectra of CS/n-HA. The peak at 1045 cm^{-1} was the overlap of the C-O-C of chitosan and the PO_4^{3-} of n-HA (stretching vibration). And the overlap of the O-H between n-HA and CS induced the blue shift. The peak at 1639 cm^{-1} was attributed to the C = N formed by schiff reaction of amino group and glutaraldehyde. The above IR spectrum analysis results show that the CS/n-HA composite microspheres contain both CS and n-HA, and no other impurity peaks appear. The infrared spectral characteristic absorption peaks of CSH/CS/n-HA composites fully illustrated the successful preparation of composites.

XRD pattern further confirmed the existence of CSH/CS/n-HA composites. The characteristic peak shape of n-HA was sharper, indicating that the crystallinity of n-HA synthesized by ultrasonic-assisted chemical precipitation was high. The above XRD pattern analysis showed that the CS/n-HA composite microspheres were further confirmed to contain both CS and n-HA components, and no other impurity peaks appeared. The phase results of CS/n-HA showed that the diffraction peak intensity of the XRD pattern was weak. Therefore, the overall intensity of the diffraction peak of the CSH/CS/n-HA composite is weakened attributed to the addition of the CS/n-HA composite.

From mechanical strength results, it is know that when the content of CS/n-HA increases to 8%,, the adhesion between the materials decreased, and the stent was more easily loosened, resulting in a decrease in the compressive strength of the sample. The in-vitro degradation illustrated that the cumulative trend of the weight loss rate of the five groups of samples showed no significant difference with time, increasing day by day, and almost completely degraded by soaking until the 15th day. Therefore, the results revealed that the CSH/CS/n-HA composite scaffolds with different CS/n-HA content are biodegradable, and the addition of CS/n-HA does not affect the degradation rate.

The results of in vitro hemolysis experiments illustrated that the suspensions of n-HA, CS/n-HA and CSH/CS/n-HA were in the range of 0.025 ~ 0.8 mg/mL, and the hemolysis rate was less than 5%. There is no hemolysis, and both meet the requirements of hemolysis experiments and national standards for medical materials. Through the above experimental research, it can be preliminarily believed that these three self-made materials will not cause acute hemolysis and have good biosafety.

3. Conclusion

The hydroxyapatite which exhibits a rod-like morphology with uniform particle size distribution and high crystallinity was successfully fabricated by ultrasound-assisted chemical precipitation method. CS/n-HA composite microspheres with rules, uniform particle size, high regularity and good dispersion were synthesized under the optional conditions (the volume ratio of water to oil phase was 1:5, the content of n-HA was 40%, the reaction temperature was 50°C, the amount of emulsifier was 0.75 mL, and the amount of crosslinking agent was 0.6 mL). The mechanical strength of CSH/CS/n-HA was higher than CS/n-HA composite microspheres, which revealed that adding the appropriate amount of CS/n-HA composite microspheres can effectively improve the maximum compressive strength of porous composite stent. When the CS/n-HA content was 6%, the compressive strength of the composite scaffold reached the highest (17.46 ± 1.29 MPa). The result of in-vitro degradation study, showed that the CSH/CS/n-HA composite scaffolds with different CS/n-HA concentration are biodegradable, and the addition of CS/n-HA does not affect the degradation rate. The Ca^{2+} concentration of soaking solution of pure CSH scaffold and the remaining four sets of composite scaffolds with different CS/n-HA content presented a decline trend with the extension of time. There was no significant difference in the trend line of change between pure CSH scaffold and the remaining four sets of composite scaffolds with different CS/n-HA content and the Ca^{2+} concentration was always higher than the SBF stock solution. Before and after degradation, the concentration of PO_4^{3-} is consistent with the concentration in the SBF stock solution, while the concentration of PO_4^{3-} in the degradation process is always lower than that of the SBF stock solution. During the body fluid soaking experiment, sediments appeared at the bottom of the beaker, which proved precipitated hydroxyapatite formed contributed to the dynamic changes of Ca^{2+} and PO_4^{3-}. The hemolysis rates of the suspension of three self-made materials, n-HA, CS/n-HA and CSH/CS/n-HA composite microsphere within the concentration range of 0.025-0.8 mg/mL are below 5%. There is no hemolysis phenomenon, and all meet the hemolysis experiment requirements and national standards of medical materials. In this paper, porous hemihydrate calcium sulfate/chitosan/hydroxyapatite composite scaffold with good biosafety was successfully prepared. Porosity is an important property of tissue engineering, which is conducive to cell adhesion and proliferation. It was implied that the CSH/CS/n-HA scaffold have potential as candidate for application in bone tissue engineering.

4. Materials And Methods

4.1 Materials

Calcium nitrate tetrahydrate, chitosan, metavanadate, molybdate were purchased from Shanghai Macklin Biomedical Technology Co., Ltd. (China). The degree of deacetylation of CS was higher than 95%. Isopropanol, ethylenediaminetetraacetic acid were obtained from Zhiyuan Chemical Reagent Factory (Tianjin, China). Span-80 was provided by Sigma Aldrich. Pentylene glycol (25%, Kemiou, Tianjin), Calcium sulfate hemihydrate (Saen, Shanghai), Diammonium hydrogen phosphate (Damo, Tianjin) were utilized to synthesis CSH/CS/n-HA. Sodium chloride injection (0.9%, purchased from Jiangxi Kelun

Pharmaceutical Co., Ltd.), Watson's distilled water (provided by Guangzhou Watson's Food & Beverage Co., Ltd.), heparinized test tube (obtained from Taizhou Huarui Medical Instrument Co., Ltd.) were used for hemolysis experiments. All chemical reagent were of analytical grade and used without further purification.

4.2 Synthesis of CSH/CS/n-HA composite microspheres

In this work, n-HA were synthesized by ultrasonic-assisted chemical precipitation method. $Ca(NO_3)_2{\cdot}4H_2O$ and $(NH_4)_2HPO_4$ were dissolved in deionized water respectively, while ammonia solution was used to adjust the pH of the solution on 10. $(NH_4)_2HPO_4$ solution was added slowly to the solution of $Ca(NO_3)_2{\cdot}4H_2O$ until the Ca/P molar ratio was equal to the stoichiometric value of n-HA (1.67) [35]. The mixture was vigorously stirred for 1 h at 40 ℃. After stirring, the suspension was dispersed by ultrasound for 45 min [36]. The sediment was removed from the suspension by centrifuge method at a rotation speed of 2000 rpm/min, then washed several times with deionized water and anhydrous ethanol, respectively. The resulting powder was dried at 80 ℃, then calcined at 700 ℃ for 2 h.

In this experiment, CS/n-HA composite microspheres were synthesized by inverse crosslinking-emulsion method. The powder was synthesized by the following procedures: (i) CS powder (0.15 g) was dissolved in 5 mL of 2% glacial acetic acid solution, subsequently 40% n-HA were added to form a homogeneous solution. (ii) The round-bottom flask containing 25 mL liquid paraffin of 3% Span-80 was stirred in a water bath at 50 ℃ to form a homogeneous solution. (iii) The chitosan solution was added drop by drop into liquid paraffin, and then stirred for 40 min at 50 ℃. (iv) Proportional glutaraldehyde was added into the mixture as crosslinking agent. (v) After 50 min of crosslinking reaction, CS/n-HA composite microspheres were obtained by centrifugation, washed several times with isopropanol, petroleum ether and anhydrous ethanol and dried at 60 ℃.The CS/n-HA composite microspheres with different properties (weight ratio, 0%, 2%, 4%, 6%, 8%) and 1% sodium bicarbonate as foaming agent were well blended with calcium sulfate hemihydrate and appropriate amount of calcium sulfate dihydrate as coagulant. The citric acid solution was used as solidifying solution, with the ratio of liquid to solid was 0.4 mL/g, and then stirred. Porous CSH/CS/n-HA composite scaffolds were prepared by pouring the mixture slurry into the self-made silica gel tubes and curing.

4.3 Characterization of materials

The structural compositions of samples were examined by FTIR (Perkin Elmer Spectrometer 100 device) analysis in the range of 4000 – 400 cm^{-1}. Scanning electron microscopy (TFSEM) were used to observe the morphology of CSH/CS/n-HA composite scaffolds. The phase and crystallinity of samples were detected using X-ray diffraction analysis (XRD, D8 Advance Diffractometer, Bruker, Germany) with 40 KV and a scanning range of 10°C to 70°C. After preparing porous CSH/CS/n-HA composite scaffolds with different CS/n-HA content, the five sets of samples were subjected to compression test using a universal tensile testing machine.

4.4 In-vitro degradation of scaffolds

Five groups of samples (pure CSH, CSH/2wt%CS/n-HA,CSH/4wt%CS/n-HA, CSH/6wt%CS/n-HA, CSH/8wt%CS/n-HA) were dried to constant weight and their initial weight M_0 were weighed. Then the samples were soaked in 50 mL simulated body fluid (SBF) and taken out to dry to constant weight M_n (n = 1, 2, 3……) every 24 h. The SBF solution was fabricated according to previous paper. The original soaking solution were replaced with fresh SBF to continue the experiment. Repeating the above steps every 24 h and calculating the daily weight loss rate (DWL%) and cumulative weight loss rate (CDWL%) of the samples. The formulas are as follows:

$DWL_n\%=(M_n-M_0)/M_0\times100\%$

$CDWL_n\%=DWL_1\%+DWL_2\%+……+DWL_n\%$

4.5 Iron release

4.5.1 Change of calcium concentration

The concentration of calcium ion in SBF solution was determined by complexometric titration of ethylenediaminetetraacetic acid (EDTA) and calculated. 30.00 mL immersion solution were taken in conical bottle and moderate 20% NaOH solution was used to adjust pH, titrating with 0.02 mol/L EDTA solution. The change of Ca^{2+} concentration in the immersion solution can be calculated according to the volume consumption of EDTA. The formula is as follows:

$$\mathrm{C_{Ca}} = \frac{\mathrm{C_{EDTA}} \times \mathrm{V_{EDTA}}}{30}$$

4.5.2 Change of phosphate concentration

The concentration of phosphate ion (PO_4^{3-}) in SBF solution was determined by UV spectrophotometry of phosphorus vanadium molybdate yellow colorimetric method. Firstly, KH_2PO_4 was accurately weighed precisely to prepared a mother liquor with PO_4^{3-} concentration of 100 μg/mL. We accurately extracted 0.0, 0.6, 0.8, 1.0, and 1.2 mL in a 25 mL volumetric flask, and then added HNO_3 solution (1:1) 0.5. mL, 0.25% ammonium citrate 0.5 mL, 5% ammonium molybdate 0.5 mL were sharked and mixed completely, finally made up to volume with deionized water. Taking the reagent blank as a control, the absorbance value was measured at 319 nm and a standard curve was drawn to obtain an equation.

Taking 1 mL of the soaking solution under daily replacement in a 25 mL volumetric flask,the concentration of PO_4^{3-} was obtained by following the above formula via measuring the corresponding absorbance value. Furthermore, the change of phosphate ion concentration in daily SBF soaking solution was calculated during degradation

4.6 Hemolysis experiment

The in vitro red blood cell hemolysis test was carried out according to the method described in the related literature [37], and the “Standard Practice for Assessment of Hemolytic Properties of Materials” from Chinese National Standards (GB/T 16886.4–2003) to evaluate the blood compatibility of the n-HA, CS/n-HA and CSH/CS/n-HA microspheres [38]. Above all, the blood of New Zealand male rabbit (Purchased from Southern Medical University Experimental Animal Center, China, SCXK2016-0041) was obtained by ear edge incision. Accurately measuring 10 mL of red blood cells into a 500 mL volumetric flask and dilute with saline to obtain 2% red cell suspension (RCS). After grinding the CSH/CS/n-HA composite scaffold into powder, the n-HA, CS/n-HA and CSH/CS/n-HA microspheres were configured as a series of sample suspensions (0.025 ~ 0.8 mg/mL) with saline. Then, 2.5 mL of the sample suspension of different concentration and 2% RCS with gently shaking and mixing were placed in a 37 ^{o}C water bath for one hour. The mixture was centrifuged at low speed, and the supernatant was collected and the absorbance was measured at 538 nm by ultraviolet-visible spectrophotometer, and parallel experiments was performed 3 times. At the same time, a negative control and a positive control group were set up. The negative control group was added with 2.5 mL of physiological saline, and the positive control group was added with 2.5 mL of Watson's distilled water. The hemolysis rate is calculated according to the following formula:

$$\mathrm{Hemolyticactivity}\,(\backslash\%) = \frac{\mathrm{A_{sample}\text{-}A_{negative\ control}}}{\mathrm{A_{positive\ control}\text{-}A_{negative\ control}}} \times 100\%$$

Where A_{sample} is the absorbance of the testing sample and $A_{negative\ control}$ and $A_{positive\ control}$ are the absorbances of the negative and positive control, respectively.

Declarations

Acknowledgments

This work is financially supported by Science and Technology Planning Project of Guangzhou Science and Technology Bureau (No.202102080365), Science and Technology Planning Project of Guangdong Science and Technology Department (No.KTP20200170), Guangdong MEPP Fund (No.GDOE[2019]A27), Yunfu City Science and Technology Plan Project (No.2020020101), Heyuan City Science and Technology Plan Project (No.2018014), Natural Science Foundation of Guangdong Province, China (No.2018A030310477) and Zhongshan Social Welfare and basic research program (No.2020B2005).

Conflict of interest

The authors wish to confirm that there are no known conflicts of interest associated with this publication.

Availability of data and materials

The datasets supporting the conclusions of this article are included within the article.

References

1. Y. Liu, D. Luo, T. Wang, Hierarchical structures of bone and bioinspired bone tissue engineering. Small **12**(34), 4611–4632 (2016)
2. S.K. Sarkar, B.T. Lee, Hard tissue regeneration using bone substitutes: an update on innovations in materials. Korean J. Intern. Med. **30**(3), 279 (2015)
3. B.F. Boyce, L. Xing, Biology of RANK, RANKL, and osteoprotegerin. Arthritis research & therapy **9**(1), S1 (2007)
4. B. Gaihre, S. Uswatta, A.C. Jayasuriya, Reconstruction of craniomaxillofacial bone defects using tissue-engineering strategies with injectable and non-injectable scaffolds. Journal of functional biomaterials **8**(4), 49 (2017)
5. X. Wang, X. Wu, H. Xing, G. Zhang, Q. Shi, E.L., … Wang, L, Porous nanohydroxyapatite/collagen scaffolds loading insulin PLGA particles for restoration of critical size bone defect. ACS Appl. Mater. Interfaces **9**(13), 11380–11391 (2017)
6. C. Szpalski, M. Wetterau, J. Barr, S.M. Warren, Bone tissue engineering: current strategies and techniques—part I: scaffolds. Tissue Engineering Part B: Reviews **18**(4), 246–257 (2012)
7. Y.P. Guo, J.J. Guan, J. Yang, Y. Wang, C.Q. Zhang, Q.F. Ke, Hybrid nanostructured hydroxyapatite–chitosan composite scaffold: bioinspired fabrication, mechanical properties and biological properties. Journal of Materials Chemistry B **3**(23), 4679–4689 (2015)
8. J. Sun, X. Zheng, H. Li, D. Fan, Z. Song, H. Ma, … J. Hui, Monodisperse selenium-substituted hydroxyapatite: Controllable synthesis and biocompatibility. Materials Science and Engineering: C **73**, 596–602 (2017)
9. H.E.F. Abd, Y.B.D.S. Helmy, B. El-Kholy, M. Marie, In vivo animal histomorphometric study for evaluating biocompatibility and osteointegration of nano-hydroxyapatite as biomaterials in tissue engineering. J. Egypt. Natl Cancer Inst. **22**(4), 241–250 (2010)
10. S. Bose, S. Tarafder, A. Bandyopadhyay, 2015. Hydroxyapatite coatings for metallic implants. Hydroxyapatite (Hap) for biomedical applications (pp. 143–157). Woodhead Publishing
11. L.F. Sukhodub, L.B. Sukhodub, O. Litsis, Y. Prylutskyy, Synthesis and characterization of hydroxyapatite-alginate nanostructured composites for the controlled drug release. Mater. Chem. Phys. **217**, 228–234 (2018)
12. Y. Huang, G. Zhou, L. Zheng, H. Liu, X. Niu, Y. Fan, Micro-/nano-sized hydroxyapatite directs differentiation of rat bone marrow derived mesenchymal stem cells towards an osteoblast lineage. Nanoscale **4**(7), 2484–2490 (2012)
13. H. Zhou, J. Lee, Nanoscale hydroxyapatite particles for bone tissue engineering. Acta biomaterialia **7**(7), 2769–2781 (2011)
14. S. Pina, J.M. Oliveira, R.L. Reis, Natural-based nanocomposites for bone tissue engineering and regenerative medicine: A review. Adv. Mater. **27**(7), 1143–1169 (2015)

15. A. Haider, S. Haider, S.S. Han, I.K. Kang, Recent advances in the synthesis, functionalization and biomedical applications of hydroxyapatite: a review. Rsc Advances **7**(13), 7442–7458 (2017)
16. A. Fihri, C. Len, R.S. Varma, A. Solhy, Hydroxyapatite: A review of syntheses, structure and applications in heterogeneous catalysis. Coord. Chem. Rev. **347**, 48–76 (2017)
17. M.H. Fathi, A. Hanifi, Evaluation and characterization of nanostructure hydroxyapatite powder prepared by simple sol–gel method. Materials letters **61**(18), 3978–3983 (2007)
18. B. Cengiz, Y. Gokce, N. Yildiz, Z. Aktas, A. Calimli, Synthesis and characterization of hydroxyapatite nanoparticles. Colloids Surf., A **322**(1–3), 29–33 (2008)
19. F. Bakan, O. Laçin, H. Sarac, A novel low temperature sol–gel synthesis process for thermally stable nano crystalline hydroxyapatite. Powder Technol. **233**, 295–302 (2013)
20. M.A. Kassem, A.N. ElMeshad, A.R. Fares, Lyophilized sustained release mucoadhesive chitosan sponges for buccal buspirone hydrochloride delivery: Formulation and in vitro evaluation. AAPS PharmSciTech **16**(3), 537–547 (2015)
21. R.A.A. Muzzarelli, C. Muzzarelli, 2005. Chitosan chemistry: relevance to the biomedical sciences. Polysaccharides I (pp. 151–209). Springer, Berlin, Heidelberg
22. K. Oungbho, B.W. Müller, Chitosan sponges as sustained release drug carriers. Int. J. Pharm. **156**(2), 229–237 (1997)
23. M. Kong, X.G. Chen, K. Xing, H.J. Park, Antimicrobial properties of chitosan and mode of action: a state of the art review. Int. J. Food Microbiol. **144**(1), 51–63 (2010)
24. P.C. Schulz, M.S. Rodriguez, D. Blanco, L.F. Pistonesi, M., & E. Agullo, Emulsification properties of chitosan. Colloid Polym. Sci. **276**(12), 1159–1165 (1998)
25. R. Jayakumar, N. Nwe, S. Tokura, H. Tamura, Sulfated chitin and chitosan as novel biomaterials. Int. J. Biol. Macromol. **40**(3), 175–181 (2007)
26. C. Shuai, C. Gao, P. Feng, S. Peng, X. Wen, Grain growth associates mechanical properties in nano-hydroxyapatite bone scaffolds. J. Nanosci. Nanotechnol. **13**(8), 5340–5345 (2013)
27. A. Muxika, A. Etxabide, J. Uranga, P. Guerrero, K. De La Caba, Chitosan as a bioactive polymer: Processing, properties and applications. Int. J. Biol. Macromol. **105**, 1358–1368 (2017)
28. I.Y. Kim, S.J. Seo, H.S. Moon, M.K. Yoo, I.Y. Park, B.C. Kim, C.S. Cho, Chitosan and its derivatives for tissue engineering applications. Biotechnology advances **26**(1), 1–21 (2008)
29. E. Khor, L.Y. Lim, Implantable applications of chitin and chitosan. Biomaterials **24**(13), 2339–2349 (2003)
30. K.J. Burg, S. Porter, J.F. Kellam, Biomaterial developments for bone tissue engineering. Biomaterials **21**(23), 2347–2359 (2000)
31. P. Wang, E.J. Lee, C.S. Park, B.H. Yoon, D.S. Shin, H.E. Kim, … S.H. Park, Calcium sulfate hemihydrate powders with a controlled morphology for use as bone cement. J. Am. Ceram. Soc. **91**(6), 2039–2042 (2008)

32. G. Lewis, Injectable bone cements for use in vertebroplasty and kyphoplasty: State-of-the-art review. Journal of Biomedical Materials Research Part B: Applied Biomaterials: An Official Journal of The Society for Biomaterials, The Japanese Society for Biomaterials, and The Australian Society for Biomaterials and the Korean Society for Biomaterials **76**(2), 456–468 (2006)
33. Z. Chen, H. Liu, X. Liu, F.Z. Cui, Injectable calcium sulfate/mineralized collagen-based bone repair materials with regulable self-setting properties. Journal of Biomedical Materials Research Part A **99**(4), 554–563 (2011)
34. E. Hughes, T. Yanni, P. Jamshidi, L.M. Grover, Inorganic cements for biomedical application: calcium phosphate, calcium sulphate and calcium silicate. Adv. Appl. Ceram. **114**(2), 65–76 (2015)
35. R.A.A. Muzzarelli, C. Muzzarelli, 2005. Chitosan chemistry: relevance to the biomedical sciences. Polysaccharides I (pp. 151–209). Springer, Berlin, Heidelberg
36. A. Haider, S. Haider, S.S. Han, I.K. Kang, Recent advances in the synthesis, functionalization and biomedical applications of hydroxyapatite: a review. Rsc Advances **7**(13), 7442–7458 (2017)
37. L. Liu, N. Li, T. Lei, K. Li, Y. Zhang, The in vitro biological properties of Mg-Zn-Sr alloy and superiority for preparation of biodegradable intestinal anastomosis rings. Medical science monitor: international medical journal of experimental and clinical research **20**, 1056 (2014)
38. Y.G. Bi, Z.T. Lin, S.T. Deng, Fabrication and characterization of hydroxyapatite/sodium alginate/chitosan composite microspheres for drug delivery and bone tissue engineering. Materials Science and Engineering: C **100**, 576–583 (2019)
39. X. Chen, Y. Liu, J. Yang, W. Wu, L. Miao, Y. Yu, … W. Sun, The synthesis of hydroxyapatite with different crystallinities by controlling the concentration of recombinant CEMP1 for biological application. Materials Science and Engineering: C **59**, 384–389 (2016)
40. R.M. Ion, D. Turcanu-Caruţiu, R.C. Fierăscu, I. Fierăscu, I.R. Bunghez, M.L. Ion, … V. Rădiţoiu, Caoxite-hydroxyapatite composition as consolidating material for the chalk stone from Basarabi–Murfatlar churches ensemble. Appl. Surf. Sci. **358**, 612–618 (2015)
41. P. Mukhopadhyay, S. Chakraborty, S. Bhattacharya, R. Mishra, P.P. Kundu, pH-sensitive chitosan/alginate core-shell nanoparticles for efficient and safe oral insulin delivery. Int. J. Biol. Macromol. **72**, 640–648 (2015)
42. G. Tripathi, B. Basu, A porous hydroxyapatite scaffold for bone tissue engineering: Physico-mechanical and biological evaluations. Ceram. Int. **38**(1), 341–349 (2012)
43. J. Chen, P. Pan, Y. Zhang, S. Zhong, Q. Zhang, Preparation of chitosan/nano hydroxyapatite organic–inorganic hybrid microspheres for bone repair. Colloids Surf., B **134**, 401–407 (2015)
44. P. Chen, L. Song, Y. Liu, Y.E. Fang, Synthesis of silver nanoparticles by γ-ray irradiation in acetic water solution containing chitosan. Radiat. Phys. Chem. **76**(7), 1165–1168 (2007)
45. R.A. Krishnan, P. Deshmukh, S. Agarwal, P. Purohit, D. Dhoble, P. Waske, … P. Dandekar, Proton play in the formation of low molecular weight chitosan (LWCS) by hydrolyzing chitosan with a carbon based solid acid. Carbohydrate polymers **151**, 417–425 (2016)

46. T. Baran, A. Menteş, Cu (II) and Pd (II) complexes of water soluble O-carboxymethyl chitosan Schiff bases: Synthesis, characterization. Int. J. Biol. Macromol. **79**, 542–554 (2015)

Figures

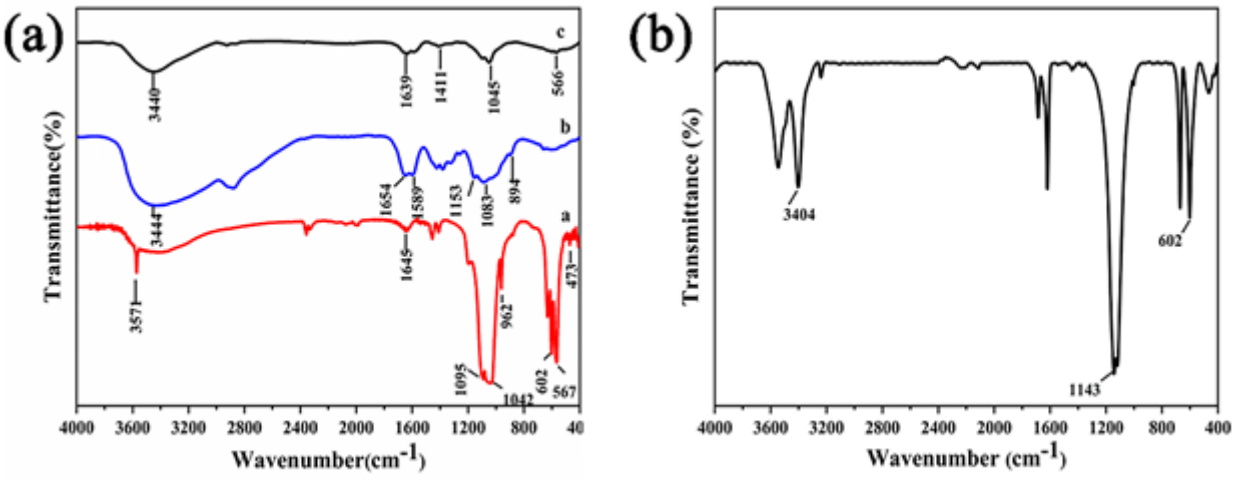

Figure 1

(a) FT-IR spectra of (a)n-HA. (b) CS. (c) CS/n-HA, and (b)FT-IR spectra of CSH/CS/n-HA

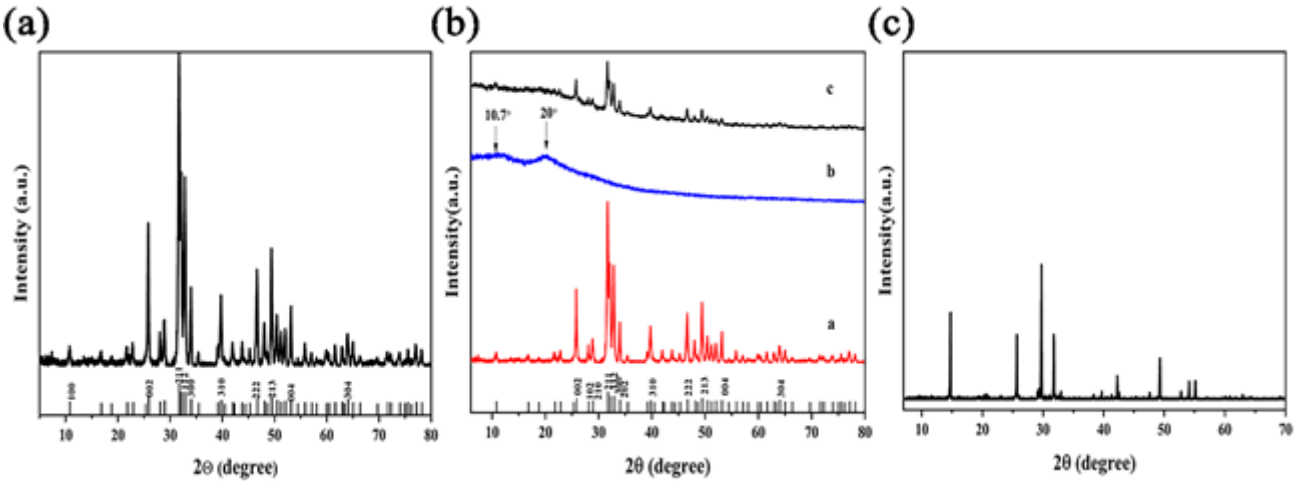

Figure 2

(a) XRD patterns of n-HA, (b)XRD patterns of (a) n-HA. (b) CS. (c) CS/n-HA, and (c) XRD patterns of CSH/CS/n-HA

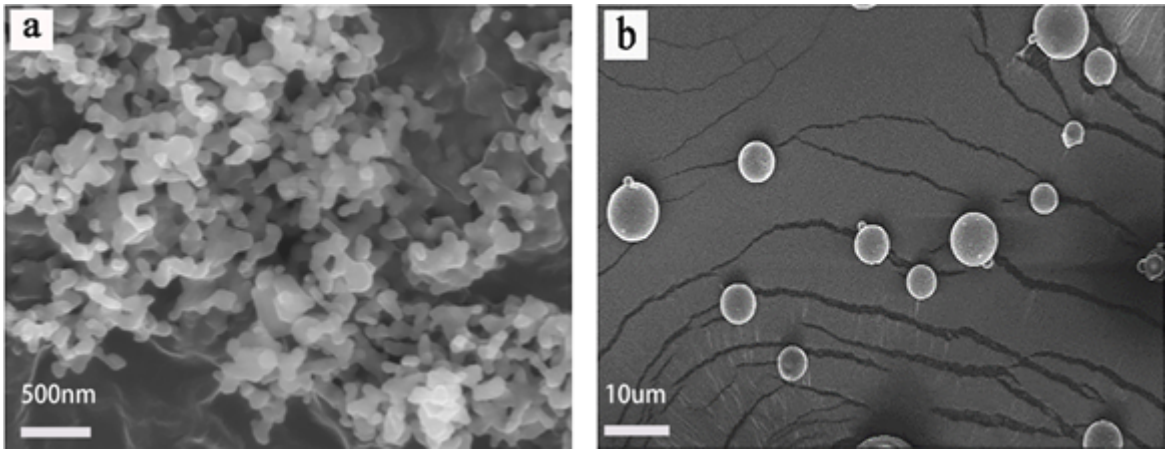

Figure 3

(a) SEM image of n-HA, (b) SEM image of CS/n-HA

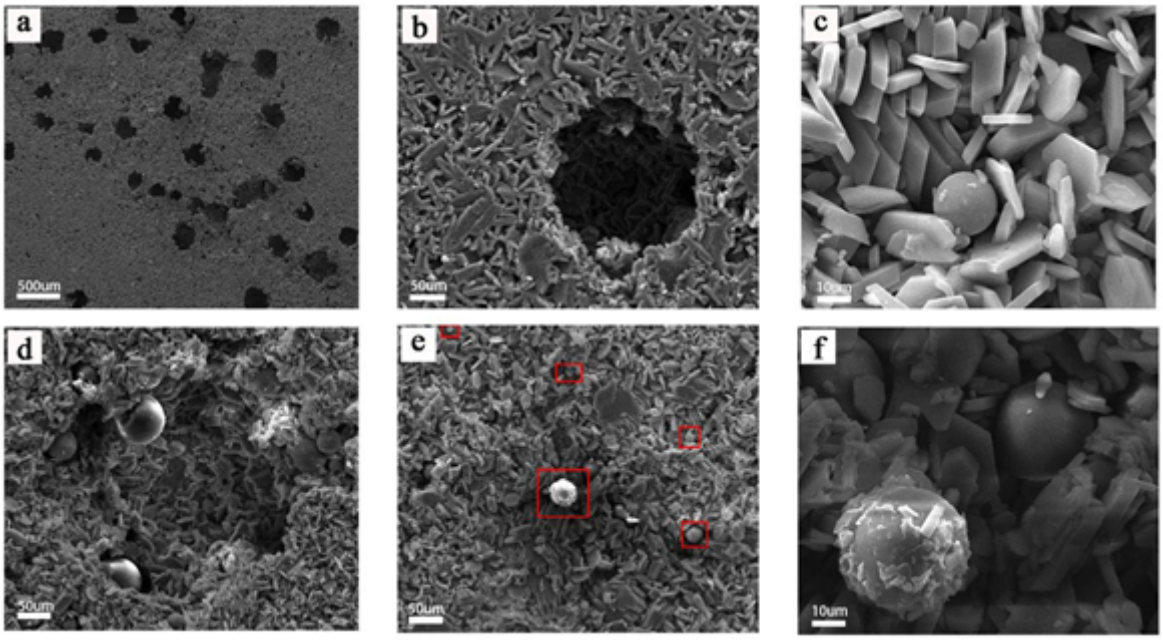

Figure 4

TFSEM image of CSH/CS/n-HA composite scaffolds

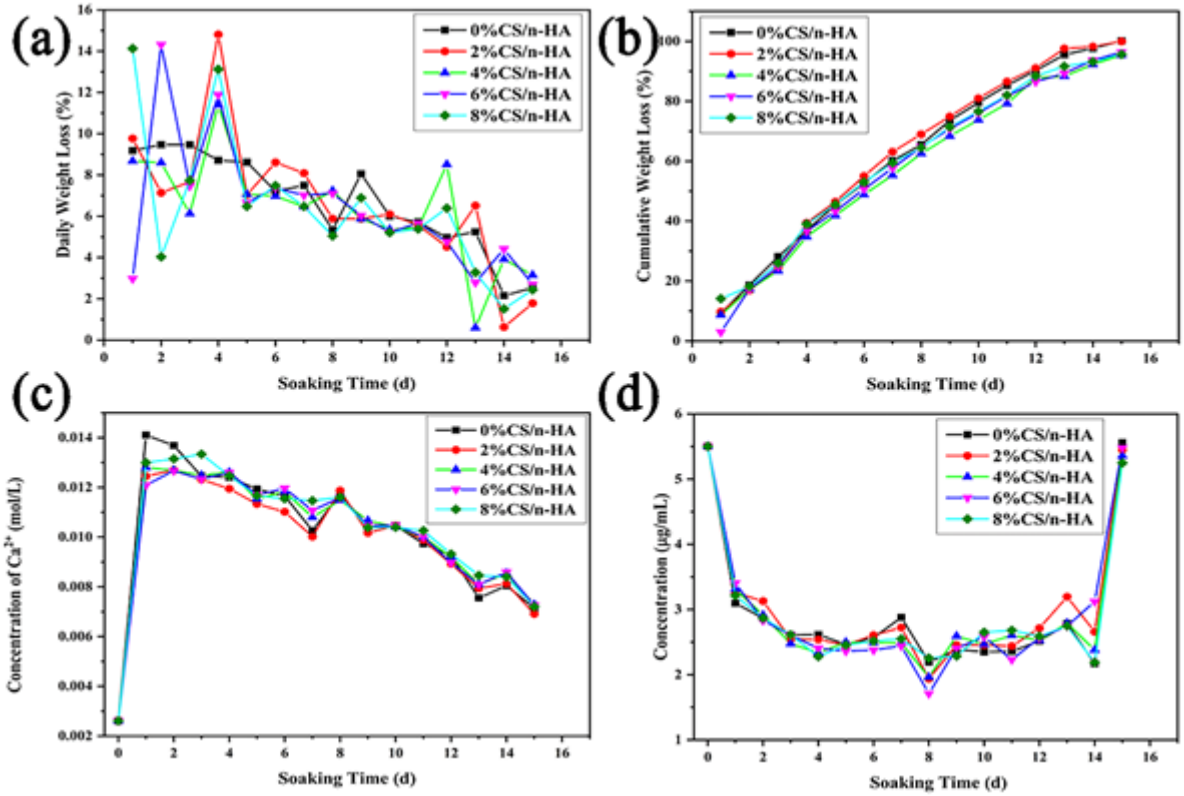

Figure 5

(a) Time trend map of daily weight loss rate of CSH/CS/n-HA composite scaffold, (b) Time trend map of cumulative weight loss rate of CSH/CS/n-HA composite scaffolds, (c)Time trend map of the concentration of Ca2+ in soaking solution, (d) Time trend map of the concentration of phosphorus element in soaking solution

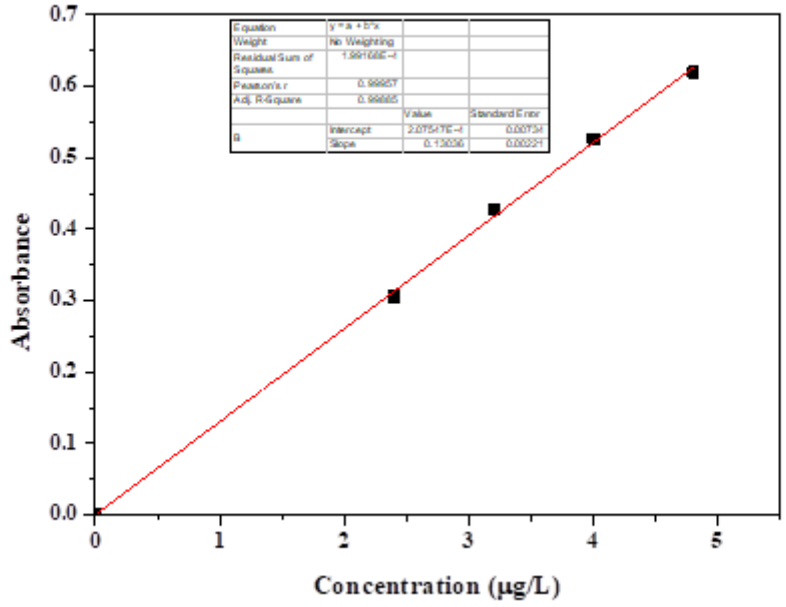

Figure 6

Standard curve of phosphorus element

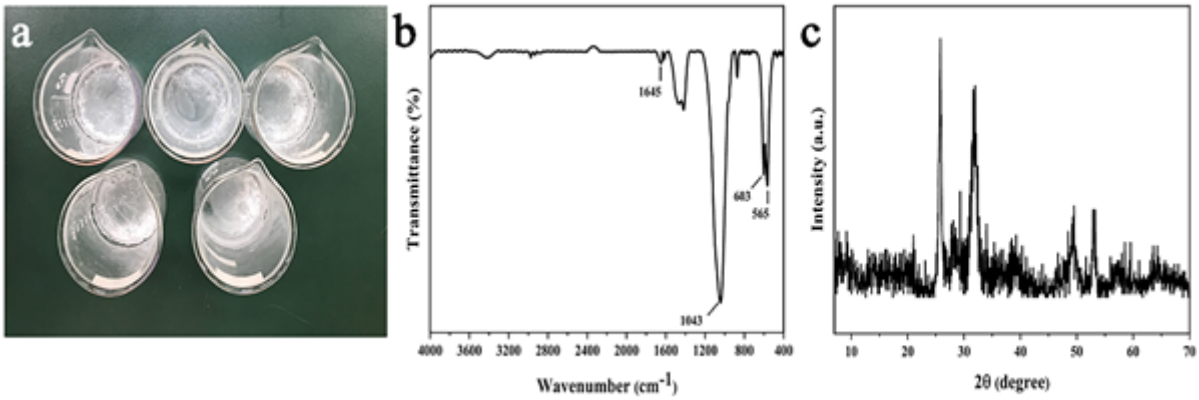

Figure 7

(a)The sediment in the bottom of flask, (b) FT-IR spectra of sediment in the bottom of flask, (c) XRD patterns of sediment in the bottom of flask

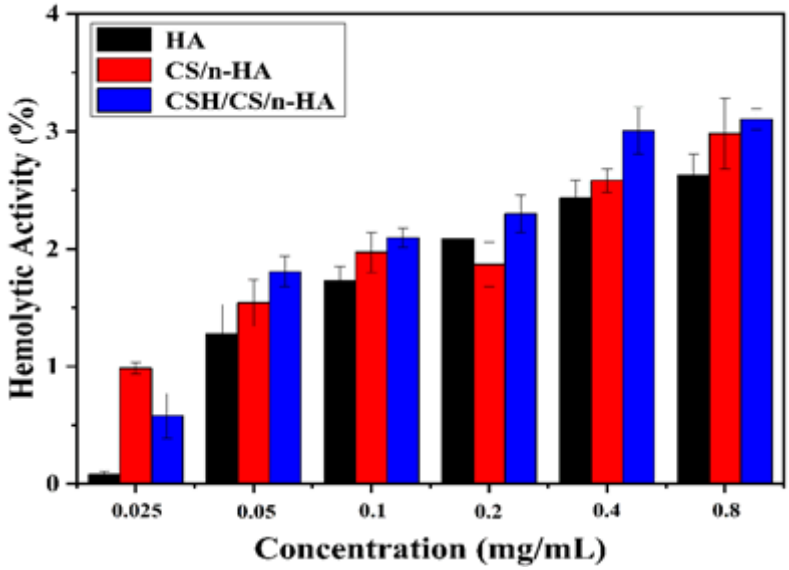

Figure 8

The result of hemolysis test